

ULTRA-RAPID LASER PROTEIN MICROPATTERNING: SCREENING FOR DIRECTED POLARIZATION OF SINGLE NEURONS

Mark A. Scott, Zachary D. Wissner-Gross, Mehmet Fatih Yanik

Supplementary Documentation

THE VARIATION OF WATER CONTACT ANGLES WITH SURFACE TREATMENTS

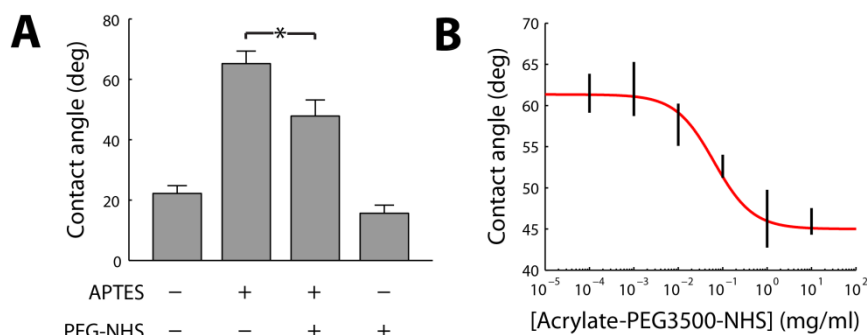


Figure S1: Water contact angle variation with addition of APTES and PEG-NHS. (a) The dependence of water contact angle with the presence or absence of APTES and PEG-NHS treatments. Error bars show \pm s.e.m. * $p < 0.05$.

To monitor the variation of surface hydrophobicity associated with the addition of a surface monolayer, the water contact angle was measured at various points during the two-step PEG-N-hydroxysuccinimide (PEG-NHS) coupling method (Fig. S1a). Nanostrip cleaned glass presented a hydrophilic surface, which became significantly more hydrophobic upon addition of 3-Aminopropyltriethoxysilane (APTES). When PEG-NHS was added, the contact angle decreased significantly, from 60° to approximately 45°. If PEG-NHS is added without first adding APTES to create a surface of amines, the contact angle remains similar to that of the plain nanostrip cleaned glass. These experiments demonstrate that APTES is a necessary intermediate for generating the PEG monolayer.

Next, to assess the bath concentration of PEG-NHS necessary to saturate the amine coated surface, we monitored the change in the surface contact angle with varying concentrations of PEG-NHS (Fig S1b). We show that the contact angle θ_c upon adding increasing concentrations of acrylate-PEG-NHS approximates (for small changes in θ):

$$\theta_c = \beta\theta_p + (1 - \beta)\theta_a$$

Where β is given by the Langmuir isotherm:

$$\beta = \frac{\alpha C_p}{1 + \alpha C_p}$$

θ_c is the water contact angle, θ_p is the contact angle measured for a PEG-2000 surface, θ_a is the contact angle measured for the aminated surface, β is the proportion of available sites that are PEGylated, C_p is the concentration of PEG solution added to the aminated surface, and α is the Langmuir constant. The contact angle suggests saturation was reached at a concentration of 10mg/ml. This concentration was used for all subsequent experiments.

SIMULATING HIGH PATTERNING SPEEDS BY MULTIPLEXING THE EOM SIGNAL BY A HIGH FREQUENCY SQUARE WAVE

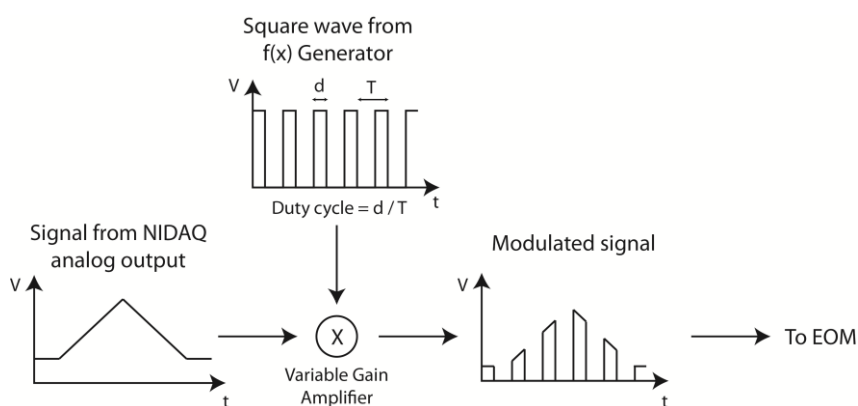


Figure S2: Electrical setup to achieve pulse-width modulation for simulating high scan speeds.

The galvanometer scanning mirrors are unable to exceed a scan speed of 10 mm/s. To simulate higher speed patterning, the signal from the NIDAQ analog output is fed into a variable gain amplifier which is gated with a 100 kHz square wave from a function generator (Fig S2). The resulting modulated signal is sent to the EOM to control the laser intensity at the B4F sample. In this manner, decreasing the duty cycle of the square wave proportionally decreases the laser dwell time, simulating a higher scan speed. For example, a physical scan speed of 10 mm/s, combined with a 1% duty cycle square wave modulating the EOM signal, simulates a scan speed of 1 m/s.

DEPENDENCE OF PATTERN BRIGHTNESS WITH FOCUS HEIGHT

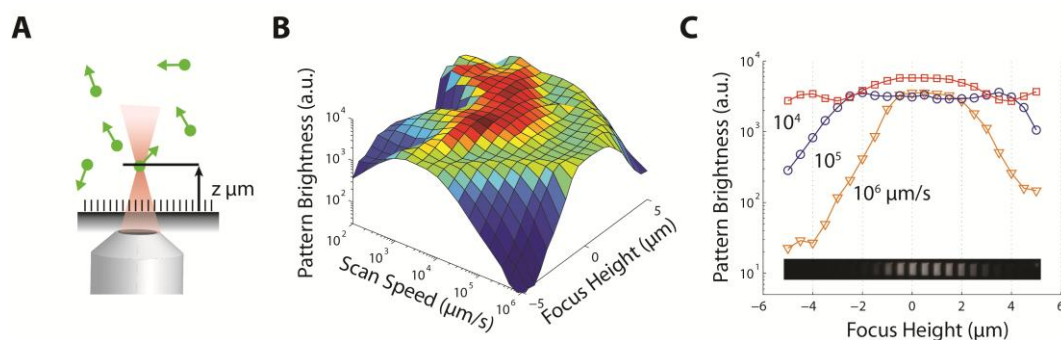


Figure S3: Variation of pattern brightness with laser focus height. (a) The focus height is defined as the height above the glass-solution interface that the laser is focused. (b) The variation in pattern brightness with scan speed and focus height. (c) The pattern brightness varies more significantly with focus height at high scan speeds. The inset image shows square patterns produced at 1 m/s at varying focus heights.

Because we are photopatterning B4F using a multi-photon process, we would expect a strong dependency on pattern brightness with focus height. To test this, we formed streptavidin patterns using a range of patterning speeds, and a laser power of 5 nJ/pulse (Fig S3). We found that at low speeds (< 10 mm/s), because the laser exposure is far above that needed for saturation (see Fig 2c, iv in the main text), the pattern brightness did not depend strongly with laser focus. However, at higher scan speeds, especially at 1 m/s, pattern brightness varies significantly with focus height. At 1 m/s, a full-width half maximum focus variation of ~ 4 μm was measured. These results emphasize the importance of using an autofocussing system for patterning large areas. Also, note the slight asymmetry about $z = 0$ μm . This is likely due to the fact that when the laser is focused above the surface, the B4F radicals can then diffuse down and bind to the aPEG3500 monolayer, whereas if the laser is focused below the surface, no B4F radicals are formed at the focal spot.

REMOVAL OF OXYGEN FROM B4F SOLUTION ENABLES FASTER LASER PATTERNING

We showed that removing oxygen from the B4F solution enabled patterning at lower powers when using a scan speed of 10 mm/s (Fig 2f in the main text). This suggested that a deoxygenated B4F solution should be able to pattern at higher speeds when using high laser powers. To test this, we showed that single 100 ns exposures (~ 8 pulses of light) are sufficient to generate patterns, with these spots significantly brighter in the deoxygenated sample than the oxygenated sample (Fig S4). This suggests that an ultra-high scan speed setup should employ deoxygenation as a strategy to enhance pattern brightness.

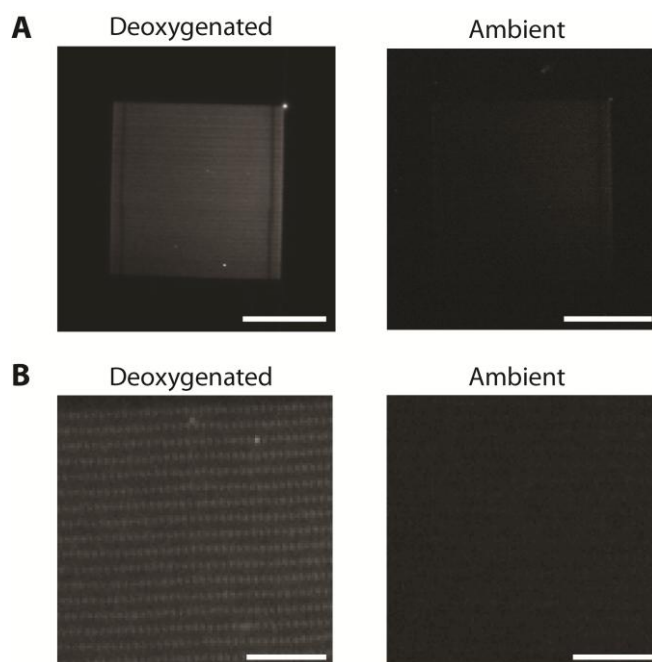


Figure S4: Removal of oxygen from the B4F solution enables bright patterning at scan speeds up to 10 m/s. (a) 100 μm square patterns formed at a simulated scan speed of 10 m/s, with and without deoxygenation of B4F. Scale bars = 50 μm . (b) Individual spots patterned with 100 ns exposure to laser light, with and without deoxygenation of B4F. Scale bars = 10 μm .

THE ADDITION OF A TRIPLET-STATE QUENCHER INHIBITS PATTERNING

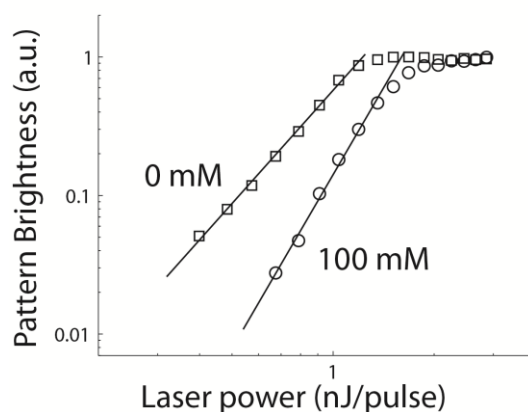


Figure S5: The addition of MEA, a triplet-state quencher, inhibits protein patterning. Patterns of streptavidin were performed at a scan speed of 10 mm/s and a laser power of 5 nJ/pulse with 0 mM or 100 mM of MEA dissolved in the B4F solution.

The strong dependence of pattern brightness on oxygen concentration (Fig S4 and Fig 2f in the main text) led us to believe that the triplet-state plays a significant role in the multi-photon photobleaching of fluorescein. To test this hypothesis, we added 100 mM of mercaptoethylamine (MEA or cysteamine) to the B4F patterning solution. We found that the MEA significantly reduced patterning efficiency, causing a significant rightward shift in the

patterning curve (Fig S5). This result is consistent with the triplet-state of fluorescein playing a significant role in the photobleaching and patterning of the fluorophore.

RELATIVE CONTRIBUTIONS OF STAGE MOVING AND SIGNAL PROCESSING TIMES TO TOTAL PATTERNING TIME

Fig S6 shows the relative contributions of laser scanning time, stage motion time, and signal processing time for patterning a $50 \times 50 \mu\text{m}$ triangle at various scan speeds. As the laser scan speed increases, the time required for signal processing (creation of scanning mirror and EOM data streams from vectorized geometric data, and uploading the data streams to the hardware NI/DAQ buffer) become increasingly rate limiting. Thus, a spinning polygonal mirror scanning system which can achieve scan speeds in excess of 1 m/s will need to be combined with methods for reducing stage motion time and signal processing time to significantly reduce total patterning time.

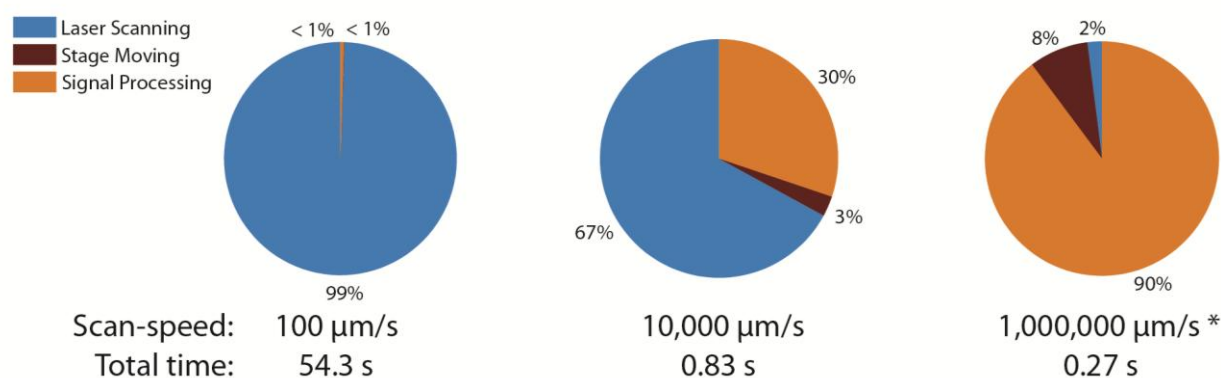


Figure S6: Distribution of total patterning time at 100 $\mu\text{m/s}$, 10,000 $\mu\text{m/s}$ and 1,000,000 $\mu\text{m/s}$ patterning speeds. Times were measured for patterning a $50 \times 50 \mu\text{m}^2$ triangle, with a scan line separation of $0.25 \mu\text{m}$. * 1,000,000 $\mu\text{m/s}$ times were projected by linearly scaling patterning time by scan speed, and by assuming stage motion time and signal processing time remain unchanged from those values measured at 100 $\mu\text{m/s}$ and 10,000 $\mu\text{m/s}$.

TIME LAPSE IMAGES OF NEURONS ON POLARIZING TRIANGLES

Fig S7 shows each of the twelve neurons used to calculate the time-averaged histogram in Fig 6c in the main text. A total of nine neurons polarized in the forward direction, and three neurons polarized in the reverse direction.

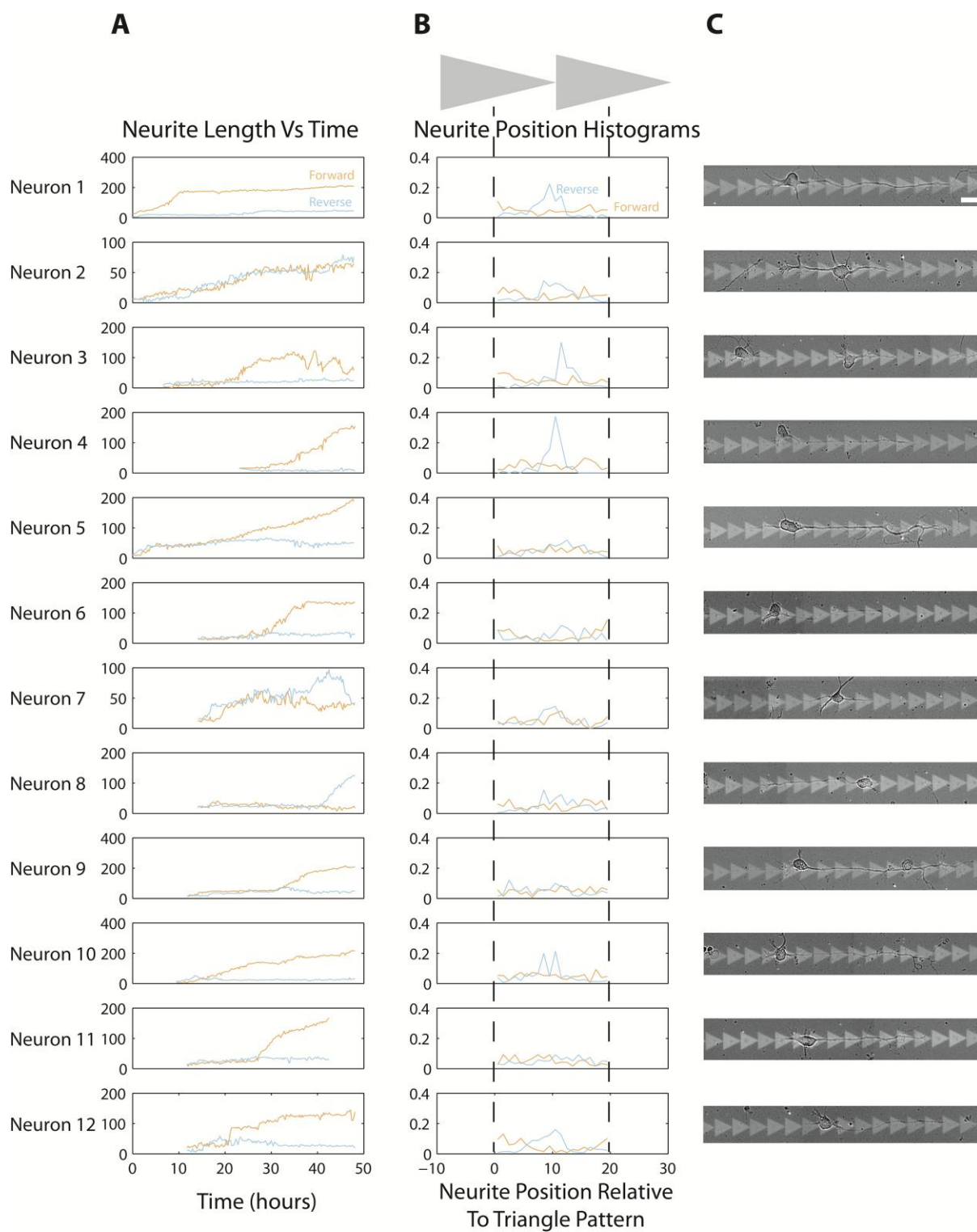


Figure S7: Time lapse length and neurite position data from multiple neurons. (a) Neurite length versus time for forward (orange) and reverse (blue) projecting neurites. (b) Neurite position histograms for forward (orange) and reverse (blue) projecting neurons. (c) Images of neurons taken at 48 h after plating. Scale bar = 20 μm .